Frequency-dependent magnetotransport and particle dynamics in magnetic modulation systems

Esmael Badran and Sergio E. Ulloa
Department of Physics and Astronomy and Condensed Matter and Surface Sciences Program, Ohio University, Athens, Ohio 45701-2979
(Received 10 August 1998)

We analyze the dynamics of a charged particle moving in the presence of spatially modulated magnetic fields. From Poincaré surfaces of section and Liapunov exponents for characteristic trajectories we find that the fraction of pinned and runaway quasiperiodic orbits vs chaotic orbits depends strongly on the ratio of cyclotron radius to the structure parameters, as well as on the amplitude of the modulated field. We present a complete characterization of the dynamical behavior of such structures, and investigate the contribution to the magnetoconductivity from all different orbits using a classical Kubo formula. Although the dc conductivity of the system depends strongly on the pinned and runaway trajectories, the frequency response reflects the topology of all different orbits, and even their unusual temporal behavior. [S0163-1829(99)01604-5]

I. INTRODUCTION

In the last few years it has become possible to build high-mobility heterojunctions with lateral surface superlattices and ''antidot'' arrays. Depending on the strength of the uniform field and the energy, the system could be considered in the quantum or classical regime, while the strength of the local potential (magnetic or electrostatic) determines whether the classical trajectories will be regular or chaotic.[1] As the lattice spacing is made much larger than the Fermi wavelength, the electron dynamics reaches a semiclassical regime. In this limit, it turns out that a competition between the classical cyclotron radius and the potential length scale (the lattice period) determines a great deal of the dynamical behavior, as we will see below. Given the great flexibility in system fabrication, it is now possible to study the full range of this problem experimentally: from the fully quantum regime to the semiclassical mechanics problem. An important example is the dynamics of ballistic electrons in a spatially modulated potential in a magnetic field, and their effect on magnetotransport.[1–3]

In the semiclassical regime, commensurability oscillations in the magnetoresistance of modulated two-dimensional electron gases have attracted much attention recently.[1] The commensurability oscillations result from the competition between two length scales: the cyclotron radius $R_c = v/\omega_o$ (where v is the particle velocity, $\omega_o = eB_o/mc$, and B_o is the applied magnetic field), and the period of the superstructure a. The case where the potential barriers are defined by an electrostatic modulation has been studied intensively both theoretically and experimentally.[1,3] The low-field oscillations in the magnetoresistance have been observed by several groups and in different regimes. For low and moderate fields (Fermi wavelength $\lambda_F \ll R_c$), and in high-mobility samples (mean free path $\ll a$), the Landau-level quantization can be neglected and a classical approach for ballistic electrons is indeed sufficient to describe the dynamics and the magnetotransport. In this regime, Wagenhuber *et al.* studied theoretically the electron dynamics in a square electrostatically-generated lattice and showed that the chaotic behavior is reflected in the low-frequency power spectrum of the system, giving rise to a peculiar type of anomalous particle diffusion.[4]

The maxima in the diagonal elements of the magnetoresistance tensor ρ_{ii} as a function of magnetic field have been attributed to the existence of pinned electron trajectories around a single maximum (or groups of them) in the potential landscape.[1] This pinning leads to a reduction in magnetoconductance σ_{ii}, with minima at fields such that $2R_c/a = n - 1/4$, where n is an integer. At the same time, the so-called runaway orbits represent skipping orbits along the rows of the potential landscape, and contribute to enhance σ_{ii}. Fleischmann, Geisel, and Ketzmerick studied the case for a square geometry by working the classical dynamics and the (zero-frequency) dc transport numerically,[3] and their results were in excellent agreement with experimental values.[1] Schuster *et al.* showed experimentally that the asymmetry of rectangular antidot superlattices is reflected in the measured dc transport, as the scattering with the antidots make the motion clearly more diffusive in one direction than the other.[5]

In this paper we investigate a model where the second length scale in the problem, apart from the cyclotron radius R_c, is defined through a periodic variation in the magnetic field itself, instead of an additional electrostatic modulation. This magnetically modulated system was introduced by Vasilopoulos and Peeters,[6] and successfully implemented by several groups.[7] In this case, it has been shown that for a weak modulation similar minima in σ_{ii} occur here but are shifted to $2R_c/a = n + 1/4$.[6] This phase shift has in fact been used to differentiate between these two effects in experiments,[7] and has been shown to persist beyond the weak modulation regime.[6,8]

For the square geometry in the magnetic modulated system, we have shown in an earlier paper that the chaotic orbits are the ones that contribute the most to the dc conductivity,[9] and reproduced the experimental results for the commensurability oscillations in the dc magnetoresistivity (similar results have been obtained by Schmidt[10]). In the (finite frequency) ac transport we showed also that the quasiperiodic (pinned) orbits give rise to resonance peaks at characteristic frequencies. In the magnetic square lattice the chaotic contribution to the ac conductivity is centered around ω_o, while

the quasiperiodic trajectories give rise to features at the frequencies associated with the rate of precession of their orbits and/or other characteristic frequencies of the motion.[9] Similar qualitative behavior has been reported in experiments by Vasiliadou *et al.* in an electrostatic square antidot array.[11] They mapped experimentally the photoconductivity signals vs the uniform field, and found a clear resonant signal related to quasiperiodic orbits around groups of (or single) antidots. These experiments are performed at low magnetic field and with frequencies in the microwave regime. Vasiliadou *et al.* found that the commensurability effects and modified classical cyclotron resonances they observed are in agreement with model calculations based on the nonlinear dynamics and classical transport of the electron.[3,11]

For the more general magnetic *rectangular* modulation, one would expect that the quasiperiodic orbits would be also reflected in the frequency-dependent magnetotransport, and reflect the system anisotropy. There are in fact three types of trajectories in this geometry: pinned and runaway *quasiperiodic*, as well as a type of runaway *chaotic*, as we will show below. This classification refers to their spatial behavior as the dynamics progresses, and it has been used to intuitively understand their contribution to the conductivity. Although the pinned quasiperiodic and runaway chaotic orbits exist in the square geometry,[9] the runaway quasiperiodic trajectory is possible only in the asymmetric modulation of a rectangular geometry, and in a regime of parameters such that the classical cyclotron orbit radius is comparable to the modulation periods. This highlights another interesting point in these systems. We show here that the electron dynamics depends only on the ratios of cyclotron orbit radius to lattice periods R_c/a, and R_c/b, and to the ratio of magnetic modulation to uniform field component $r=B_m/B_o$. We can therefore say that the chaotic character of the dynamics is controlled not only by the modulation amplitude, as one would expect, but by the size of the cyclotron orbit radius. This is somewhat different to the near independence on cyclotron radius described by Wagenhuber *et al.* in the square lattice electrostatic case.[4]

We also find, as will be discussed in Secs. III and IV below, that the chaotic orbits in the rectangular lattice differ markedly from the square lattice case, depending on the value of the ratios R_c/a and R_c/b. This leads to contributions to the ac conductivity much different than in the case of the square lattice, as unstable quasiperiodic orbits embedded in the dynamics dominate $\sigma_{ii}(\omega)$ even in a fully chaotic regime. Finally, we show in this paper that there is a direct correlation between the largest Liapunov exponent of the chaotic trajectory and σ_{ii}. The Liapunov exponent provides a direct measure of the diffusion of the particle in the chaotic orbits, even overwhelming the remnant impurity scattering (which otherwise provides a low-frequency cutoff in the power spectrum and yields normal particle diffusion).

II. MODEL AND APPROACH

Consider a 2DEG in the xy plane with a spatially modulated magnetic field, giving rise to a smooth and infinitely extended ''magnetic antidot potential.'' Perhaps the simplest form of this modulation can be described by the following expression (easily generalizable by adding more Fourier components, for example),

$$\mathbf{B}=\hat{z}B_o\left[1+\frac{r}{2}\left(\cos\frac{2\pi x}{a}+\cos\frac{2\pi y}{b}\right)\right], \tag{1}$$

where $r=B_m/B_o$ is the ratio of modulation and uniform field components ($r\leqslant 1$), and a and b are the periods of modulation along the two directions. This system can be described by the Hamiltonian $H=[\mathbf{p}+(e/c)\mathbf{A}(\mathbf{r})]^2/2m$, where m is the electronic effective mass (in GaAs, for example, the system of choice in typical experiments) and $\mathbf{A}$ is the vector potential. Choosing a symmetric gauge, this can be written as,

$$\mathbf{A}=\left(-B_o\frac{y}{2}-\frac{B_m}{2k_y}\sin k_y y, B_o\frac{x}{2}+\frac{B_m}{2k_x}\sin k_x x, 0\right), \tag{2}$$

where $k_x=2\pi/a$, and $k_y=2\pi/b$. The trigonometric functions in the Hamiltonian lead to a nonlinear coupling in the classical equations of motion. This coupling is proportional to the dimensionless quantity r, and no analytical solution can be given in general. We study the dynamics of the system by carrying out accurate numerical solutions of the equations of motion, and use Liapunov exponents to characterize the type of trajectory and their contribution to the conductivity of the system. Although the resulting equations can be solved in a linearized form for small r, this solution loses validity rather quickly as r increases. Only the numerical solutions are presented here.

In calculating the ac conductivity we use a classical version of the linear response theory (Kubo formula)

$$\sigma_{\mathrm{ij}}(\omega)\propto\int_0^\infty dt e^{-t/\tau}\ e^{i\omega t}\ \langle V_i(t)V_j(0)\rangle, \tag{3}$$

where $\langle V_i(t)V_j(0)\rangle=N_{ic}^{-1}\Sigma_{ic}V_i(t)V_j(0)$ plays the role of the velocity autocorrelation function, and the characteristic ensemble average has been substituted by an average over initial conditions (ic) in this four-dimensional phase space $\{\vec{r}_o,\vec{v}_o\}$. [Since we are only interested in the frequency dependence and magnetic field features of the conductivity, we ignore an overall normalization prefactor in Eq. (3).] Here, N_{ic} is the total number of initial conditions used, and τ is a phenomenological scattering time associated with the remnant random impurity and alloy scattering in the real system.[12] We calculate the velocity correlation function $\langle V_{\mathrm{i}}(t)V_{\mathrm{j}}(0)\rangle$ by generating random sets of initial conditions $\{\vec{r}_o,\vec{v}_o\}$, while keeping the energy constant. We can then separate the initial conditions that yield pinned and runaway orbits by using the Poincaré surface section to classify trajectories for such energy. This is accomplished by introducing a ''diffusion length,'' $d=[(x_f-x_o)^2+(y_f-y_o)^2]^{1/2}$, where (x_o,y_o) is the initial position, and (x_f,y_f) is the position at the end of the integration at time t_f ($\gg\omega_o^{-1}$). The orbit is classified as runaway if $d>qR_c$, for $q>5$, say. We use these initial conditions to generate the Poincaré surface section anew and verify whether the trajectory is indeed runaway-chaotic or runaway-quasiperiodic, for example. By identifying the pinned vs runaway trajectories, we can then directly and quantitatively correlate their characteristic frequencies with their contribution to the total transport coefficients, as we describe below. Clearly, the precise cutoff

value of q above would affect results, but only very slightly quantitatively, and not our conclusions.

Notice that in this Hamiltonian system the kinetic energy is a constant of motion, since only magnetic fields are applied. One can define the cyclotron radius $R_c = v/\omega_o = \sqrt{\dot{x}^2+\dot{y}^2}/\omega_o$ as an auxiliary length scale. Using this, the classical equations of motion can be scaled in time and length by $x/R_c \to \tilde{x}$, $y/R_c \to \tilde{y}$, and $\omega_o t \to \tilde{t}$. The equations then appear as those for two nonlinear coupled pendula,

$$\ddot{\tilde{x}} = -\dot{\tilde{y}}\left[1+\frac{r}{2}(\cos k_a\tilde{x}+\cos k_b\tilde{y})\right],$$

$$\ddot{\tilde{y}} = +\dot{\tilde{x}}\left[1+\frac{r}{2}(\cos k_a\tilde{x}+\cos k_b\tilde{y})\right], \tag{4}$$

where $\dot{\tilde{x}} = d\tilde{x}/d\tilde{t}$, etc., $k_a = 2\pi R_c/a$, and $k_b = 2\pi R_c/b$. This scaling shows the explicit dependence of the motion on only three parameters: r (magnetic field modulation amplitude), R_c/a, and R_c/b, which then fully characterize the dynamics, as we will show in the next sections.

III. POINCARÉ SURFACES OF SECTION AND LIAPUNOV EXPONENTS

Since energy is conserved in this system, the dynamics takes place on a three-dimensional ''slice'' of the phase space available. We can fully characterize the types of trajectories by means of Poincaré surfaces of section on the xy plane for a given value of velocity (or ''phase''), such as $\dot{x}$ maximum (and $\dot{y}=0$). Due to the translational symmetry of the superstructure potential in the xy plane, we fold all Poincaré sections such that the x values lie in the interval $(-a/2,a/2)$, and the y in $(-b/2,b/2)$. The phase space trajectories are uniquely determined by points in the surface of section.

We calculate Liapunov exponents by using the method of Wolfe.[13] We choose base 2 in calculating exponents, such that the distance between two nearby trajectories is $d(t) = d_0 2^{\lambda_i t}$, where λ_i are the Liapunov exponents. For a Hamiltonian system, $\Sigma_i \lambda_i = 0$, since the volume in phase space is conserved by Liouville's theorem.[14] For a given set of parameters r, R_c/a, and R_c/b, the type of trajectory depends only on the initial conditions $(\vec{r}_o, \vec{v}_o)$, as described above.

For a certain modulation strength r, we find that the fractions of runaway chaotic, runaway quasiperiodic, and pinned quasiperiodic orbits in phase space depend only on the length ratios R_c/a, and R_c/b, but not on the energy nor the uniform field individually. This dependence, consequence of the scaling shown in Eq. (4), is reflected on the ac conductivity as well. For example, in the case of a square lattice case, a Poincaré surface section and three different traces of $\sigma_{xx}(\omega)$ are shown in Fig. 1, where $r=0.6$ and $2R_c/a=1.4$ are kept constant. These traces were produced changing the energy such that $v = 0.7\omega_o a$, while the corresponding uniform field is given by $\omega_o\tau = 1.5$, 2.25, and 3.0 ($\tau = 3\times10^{-12}$ sec). In this situation, we find that the Poincaré sections do not change, and the traces of conductivity have the same features, except for a frequency shift towards ω_o, and a different amplitude. The horizontal shift in Fig. 1(b) is nothing but

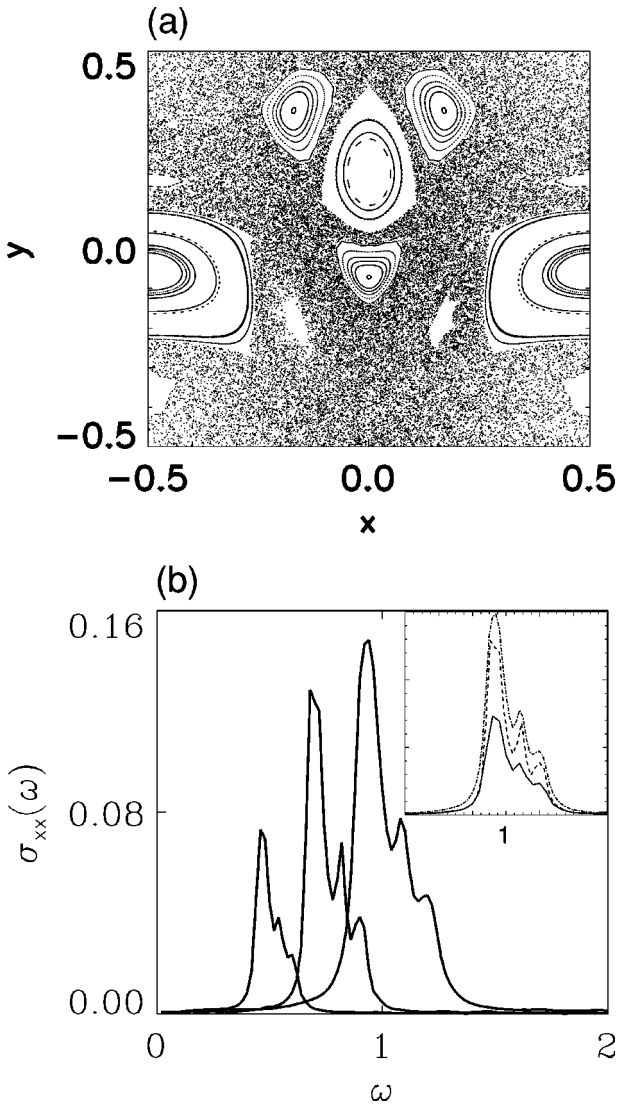

FIG. 1. (a) Poincaré surface of section for square modulation with $2R_c/a = 2v/\omega_o = 1.4$ and $r=0.6$. (b) $\sigma_{xx}(\omega)$ for the same parameters but different energy (v) and magnetic field (ω_o). Frequency ω in units of 10^{12} Hz. Inset: traces rescaled to ω/ω_o show perfect nesting.

the scaling of the frequency (or time) by ω_o (or ω_o^{-1}). The amplitude change can be understood if one analyzes the expression for the conductivity in a *uniform* field, giving the classical Drude peak with half-width $1/\tau$,

$$\sigma_{xx}(\omega) \propto \frac{\tau v^2}{1+(\omega-\omega_o)^2\tau^2}. \tag{5}$$

It is clear from this expression that the conductivity amplitude depends on the energy (via v^2). In our case of a modulated field, $\sigma_{xx}(\omega)$ shows more structure, and it appears at the expense of the Drude peak. Rescaling of the frequency to ω/ω_o in each trace produces the nesting one would expect from the scaling of Eq. (4), as clearly shown in the inset of Fig. 1(b). As we will explore further in the next section, the various features observed in these traces are contributions

from the different quasiperiodic regions in the Poincaré map, while the contribution of the chaotic region is centered close to ω_o.[9]

As explained, the characteristic size of the cyclotron orbits with respect to the magnetic lattice dimensions determines the resulting dynamics and the overall properties of the trajectories for different initial conditions. We can then consider different regimes: *First*, when $2R_c \leqslant a \leqslant b$, most orbits are localized between or around modulation maxima (single ''antidots''), as the high magnetic field (and/or low energy) effectively shrinks the electronic orbits to be fully within a period of the modulation. *Second*, when $a \leqslant 2R_c \leqslant b$, the asymmetry of the potential landscape is expected to be strongly reflected in the dynamics and transport, since all length scales are comparable and their competition produces strong changes in the dynamics. *Third*, for low magnetic fields (and/or high energies), when $a \leqslant b \leqslant 2R_c$, the lattice asymmetry becomes less and less important, as the trajectories extend over several periods of the potential landscape. Here, the particle motion effectively performs a self-averaging of the different magnetic field amplitudes, which cancels the asymmetry of the system, and yields a relatively large dc conductance and a featureless and broad frequency-dependent $\sigma(\omega)$.

For the *first regime*, consider $2R_c/a = 3/8$ and $b/a = 1,2$. Since $2R_c$ is much smaller than a and b, the electron is able to trace out periodic and quasiperiodic orbits which remain basically pinned about a lattice position, even for a high modulation r. These orbits show a variety of frequencies that can be seen in the structure of the Poincaré section. For example, when $b/a = 1$, $r = 0.6$, the Poincaré section is mostly dominated by large sectors of quasiperiodic orbits, even though the nonlinear coupling (via r) is somewhat high. We show in Fig. 2(a) that two different regions of pinned orbits exist in this portrait, surrounded by Kolmogorov-Arnold-Moser (KAM) islands of stability,[14] and a small chaotic region showing diffusion along both directions. For the chaotic orbit in this case we calculate the largest Liapunov exponent to be $\lambda = 0.85$ (while for the quasiperiodic orbits $\lambda_i \approx 0$ — this is the same for all the cases below, as anticipated, so that we will only quote the largest Liapunov exponent in the chaotic orbit from here on). The quasiperiodic structures in the Poincaré map, as we will see later, will give rise to resonance peaks in the ac conductivity.

Figure 2(b) shows a Poincaré section where $b = 2a$ and $r = 0.6$. In this case, phase space has more structure due to the asymmetry of the potential landscape, KAM islands are still well developed, and the chaotic region is larger. In this case, the largest Liapunov exponent is $\lambda = 0.91$, indicating that the motion in the chaotic regime has become more diffusive (and still two dimensional).

In the *second regime*, we consider as examples $2R_c/a = 1.2$, and $b/a \geqslant 3$ (smaller values of b/a yield results quite similar to the square geometry discussed before[9]). Since $2R_c$ is between both a and b, there is a preferred direction to the electron motion, in this case the x direction. We have shown in previous work that in the square geometry, when $2R_c \approx a = b$, the electron dynamics shows a great deal of chaotic behavior *even when the modulation constant r* is small.[9] This can be understood as being due to the fact that the electron is more likely to ''collide'' in this regime with the maxima in the modulation landscape. These collisions allow the particle to access stronger nonlinear terms in the equation of motion, which in turn produces a more critical dependence to initial conditions and then chaotic dynamics.[15]

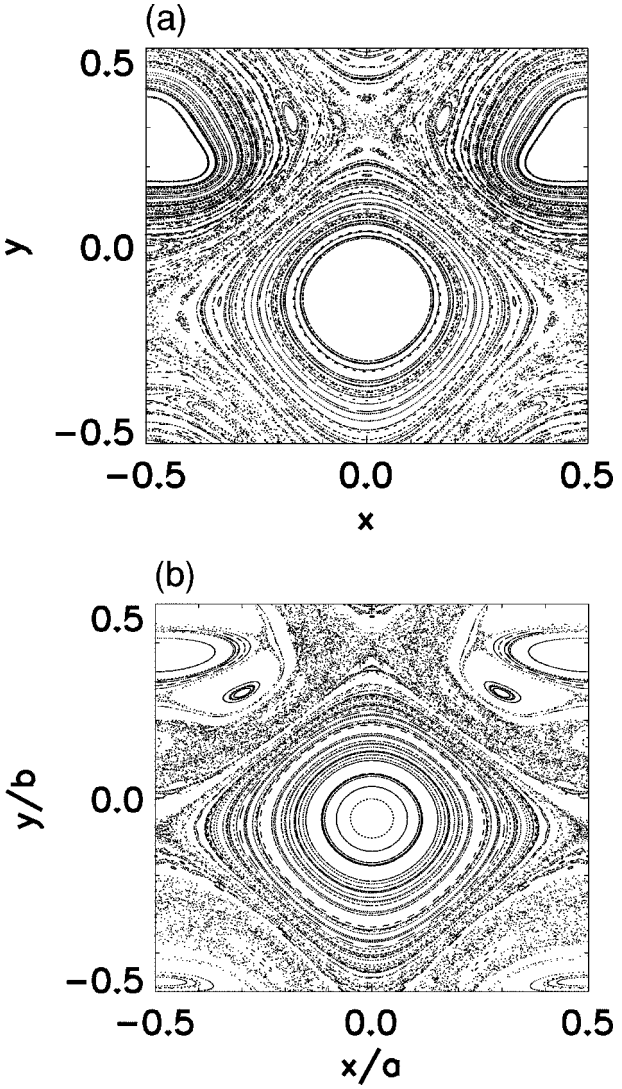

FIG. 2. Poincaré surfaces of section for the same energy, with $2R_c/a = 3/8$ and $r = 0.6$. In (a) $b = a$, while in (b) $b = 2a$.

For $b/a \gtrsim 3$, as we turn on the modulation, we notice the appearance of two kinds of quasiperiodic orbits (pinned and runaway), even for $r \lesssim 0.35$. The runaway quasiperiodic orbits result from the strong x-y asymmetry of the potential, which forces the electron to move preferentially along the x direction (smaller period). However, the modulation field is not sufficiently strong to make the electron motion chaotic, and the runaway orbits are nearly free in the preferred direction. As r increases to ≈ 0.4, the chaotic orbits start to occupy a non-negligible volume in phase space, and the largest Liapunov exponent becomes positive. In Fig. 3 we show Poincaré sections for $2R_c/a = 1.2$ and $b/a = 4$, for both $r = 0.45$ and $r = 0.85$. In Fig. 3(a), r smaller, we see three types of trajectories: two quasiperiodic (one pinned and one runaway or open), and a chaotic runaway. Notice that the chaotic trajectories are confined between two sets of quasiperiodic runaway orbits and yield then particle diffusion *only along one dimension.* In this case, the chaotic trajectories

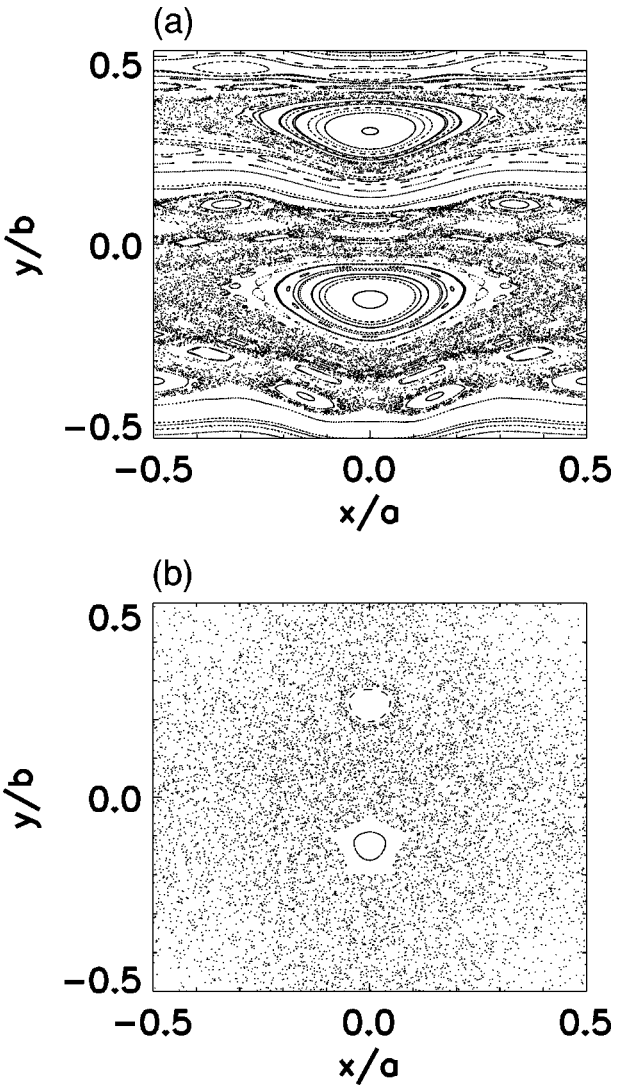

FIG. 3. Poincaré surfaces of section for the same energy, and $2R_c/a=1.2$, and $b=4a$. For (a) $r=0.45$ and (b) $r=0.85$. Notice x-direction one-dimensional diffusion of chaotic orbits in (a) evolves into two-dimensional diffusive motion in (b).

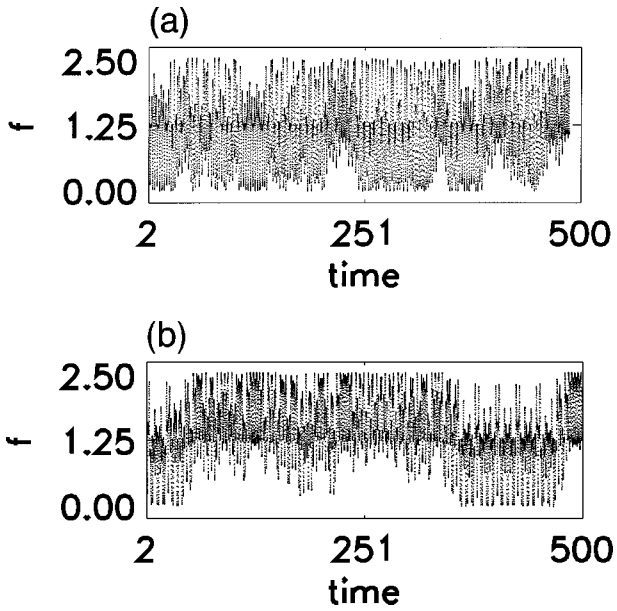

FIG. 4. Time series of the ''instantaneous frequency'' $f=eB(\mathbf{r})/mc$ that particle experiences in a chaotic trajectory. Here, $\omega_o=1.25$ ($\times 10^{12}$ Hz), while $2R_c/a=1.2$ and $r=0.85$. In (a) $a=b$, while in (b) $b=4a$. Time axis is labeled by the integration step index.

have a single characteristic frequency around ω_o, with largest Liapunov exponent $\lambda=0.98$. In Fig. 3(b), as r is nearly doubled, we see that there are two small regions of pinned quasiperiodic orbits with Liapunov exponents converging to zero individually, while the rest of phase space is filled by a chaotic orbit with largest Liapunov exponent $\lambda=1.1$, which clearly shows diffusion in two dimensions. The modulation is so strong that there are no remnants of the runaway quasiperiodic trajectories. This y-axis ''delocalization'' is similar to the energy dependence described by Wagenhuber *et al.*[4] for a symmetric electrostatic modulation case. Notice here, moreover, that energy is kept constant, via $2R_c/a$, and that the transition is produced then by the stronger modulation amplitude.

We find furthermore that the chaotic trajectories are qualitatively different in this second regime from those in the first high-field regime. In the latter, when $2R_c \leqslant a \leqslant b$, the characteristic frequency of the chaotic trajectory is always near ω_o, as the trajectory effectively samples a significant range of field values during its two-dimensional diffusion and self-averages to ω_o. In the second regime, however, we find that it is typical to find *two* characteristic frequencies embedded in the chaotic orbit at $\omega_\pm \approx \omega_o \pm \delta$, where δ increases as either b/a or r increase. This type of remnant two-frequency trajectory is produced by the asymmetry of the potential, and one can clearly see this effect in the special cases where $2R_c \approx a \ll b$, for example. These dimensions create a landscape where the electron can move for a relatively long time in the x direction in a region of fields lower than B_o (in essence a diffusive motion of its precession center), corresponding to a frequency $\omega_- \approx \omega_o - \delta$. When the motion drifts in the y direction, the electron faces a wall of maxima separated by a distance $a \approx 2R_c$, which often confines the trajectory to a region of higher fields between two maxima and pins the particle to precess for a time with characteristic frequency motion of $\omega_+ \approx \omega_o + \delta$, until it escapes again to a lower field region in the potential. The persistence of these characteristic frequencies embedded in the chaotic motion provides a unique $\sigma_{ii}(\omega)$, as we will see in the next section.

Another form of exploring this intermittence effect is by analyzing the field experienced by the particle along its chaotic trajectory. In Fig. 4 we show the ''instantaneous frequency,'' $f=eB(\mathbf{r})/mc$, which the electron experiences in the magnetic potential landscape as it moves through positions $\mathbf{r}(t)$. When $a=b$, Fig. 4(a) shows that this instantaneous frequency f varies around $\omega_o (=1.25\times 10^{12}$ Hz here) nearly uniformly. In the second plot, Fig. 4(b), the particle's instantaneous frequency spends a significant amount of time at values averaging clearly higher than ω_o, and then, in the next segment of the time series, its average is lower than ω_o. This persistent intermittent switching behavior, which continues for as long as we have run the simulations, indicates that the particle is metastably trapped in the different regions of the periodic potential, even though the trajectory is clearly chaotic, as judged by the corresponding Poincaré phase por-

trait. We will show in the next section that this kind of trajectory will give rise to two prominent peaks in the ac conductivity, even though its Poincaré map shows a typical chaotic trajectory, and one would naively expect a featureless $\sigma(\omega)$ (which is the case for $2R_c/a \gg a,b$, for example). Therefore, the peculiar metastable character of the nearly trapped sections embedded in this chaotic trajectory shows clearly in the frequency dependent conductivity.

Finally, for the low-field *third regime*, we consider $2R_c/a=6$, $b/a=2$, and $r=0.56$. Since $2R_c \gg a,b$, the electron is more likely to collide with potential maxima here than in the previous two cases, as discussed earlier, and hence chaotic orbits occupy most of phase space even for extremely low modulation (not shown). In all these cases, the chaotic orbits have an average characteristic frequency at $\omega \approx \omega_o$, but with a rather broad distribution, as we will see below. Moreover, the largest Liapunov exponent for the chaotic orbits is $\lambda = 1.14$, the largest exponent we ever obtained in all cases, indicating that the motion is indeed fully diffusive in two dimensions. This behavior will be clearly reflected on the magnetotransport described in the next section.

IV. MAGNETOTRANSPORT

A quantitative theory of magnetotransport requires detailed consideration of regular and/or quasiperiodic (pinned or runaway) and chaotic (runaway) trajectories arising from modulation scattering. In Hamiltonian systems, where the volume in phase space is conserved, the conductivity tensor σ is obtained from the sum of the individual contributions of trajectories weighted by their volume in phase space. We have shown in previous work that the contribution of pinned orbits to the dc conductivity is negligibly small, in agreement with previous work,[3] while they are closely related to peaks in the ac conductivity. We assume here that the proportion of pinned to runaway orbits does not change qualitatively even after the inclusion of impurity scattering, which should not be far from being the case if mobility in the unmodulated system is high.[12]

For the calculations of the ac conductivity we used random sets of initial conditions (typically a few thousands), and classified the orbits by inspecting the corresponding Poincaré sections, as described above. We are then able to separate the initial conditions that give rise to pinned or chaotic orbits, and clearly identify their different contributions to σ and ρ. When the modulation strength r is zero, the ac conductivity yields the classical Drude peak, as the charge experiences a uniform field and only impurity scattering, included here through τ [see Eq. (5)]. Once the magnetic modulation is turned on, however, the Drude peak remains centered around $\omega=\omega_o$, for small r, but the conductivity begins to acquire a nonhomogeneous broadening, and $\sigma_{xx}(\omega)$ and $\sigma_{yy}(\omega)$ start deviating from each other if $b \neq a$, in general. This inhomogeneous broadening appears *before* the chaotic orbits appear (r small), i.e., when the Poincaré sections show only quasiperiodic orbits. This broadening is then clearly associated with the fact that most of the electron trajectories have still the characteristic frequency ω_o. However, due to the small modulation, the electron orbits precess with characteristic frequencies which appear close to or far from ω_o, depending on structural parameters.

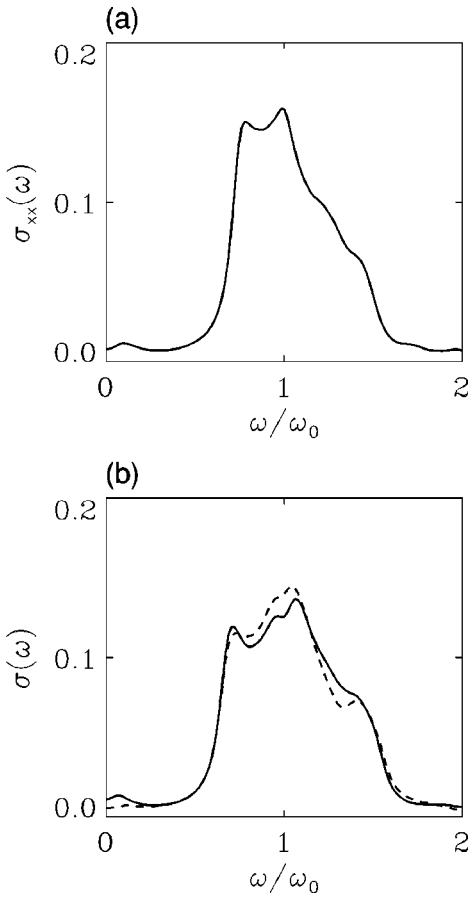

FIG. 5. Frequency-dependent conductivities, $\sigma(\omega)$. Parameters in (a) are $2R_c/a=0.4$, $b/a=1$, and $r=0.6$, and $\sigma_{xx}=\sigma_{yy}$. In (b) same parameters, except for $b/a=2$. Here, solid (dashed) line shows σ_{xx} (σ_{yy}).

By increasing the modulation strength, additional features appear in $\sigma(\omega)$ at the same time that chaos and KAM islands appear in the Poincaré surface section. Moreover, an offset at zero frequency appears in both $\sigma_{xx}(0)$ and $\sigma_{yy}(0)$ due to the onset of chaotic orbits and associated particle diffusion. An increasing portion of chaotic trajectories as r increases makes the zero offset increase at the expense of the resonance peaks. This signals the increase in dc conductance and drop in resistance produced by the magnetic modulation which has been measured in experiments on these and related systems.[1,7] We should also mention that the dc magnetoresistance calculated here shows the well-known Weiss oscillations seen recently for magnetic modulation,[7] as we have shown in Ref. 9.

In this section, we discuss the magnetoconductivity for the same three regimes of R_c/a, R_c/b, and r parameter values reviewed in the previous section. We discuss the calculated conductivity tensor components, and their relation to features of the corresponding Poincaré section for those parameter values. For the *first regime*, where $2R_c < a \leqslant b$, we have used the same initial conditions and parameters we used to generate the Poincaré surface of section in Fig. 2(a). Figure 5 shows the ac conductivity for both $b=a$ and $b=2a$. In Fig. 5(a), since $a=b$, we obviously find $\sigma_{xx}(\omega)=\sigma_{yy}(\omega)$. The $\sigma_{xx}(\omega)$ curve has two main features around ω_o, related to the two regions of quasiperiodic trajectories in the Poincaré surface of section in Fig. 2(a) which dominate the phase

space. The central feature with frequency $\omega \approx \omega_o$ is enhanced by the contribution of the small chaotic region which provides frequencies closely peaked at around ω_o. Since $2R_c/a = 3/8$ here, we see that the effect of the modulation on $\sigma(\omega)$ is relatively minor, even for the not so small $r = 0.6$, producing particle precession around the minima and maxima of the modulation landscape, in addition to some higher frequency trajectories associated with pinning near maxima.

In Fig. 5(b) we use the same parameter set used to generate the Poincaré section in Fig. 2(b). Since here $a \neq b$, the symmetry is broken and it is the case that $\sigma_{xx}(\omega) \neq \sigma_{yy}(\omega)$. By comparing the Poincaré sections in Figs. 2(a) and 2(b) we see that most of the quasiperiodic orbits in the central section survive, which in Fig. 5(b) produce the persistence of the feature in $\sigma_{xx}(\omega)$ and $\sigma_{yy}(\omega)$ at $\omega \approx 1.4\omega_o$. On the other hand, the other sector of quasiperiodic orbits does shrink and becomes surrounded by KAM islands in Fig. 2(b). Correspondingly, we see that the conductivity feature at $\omega \approx 0.8\omega_o$ becomes smaller, due to the shrinking of phase space volume occupied by these trajectories, and moves to lower frequencies ($\approx 0.6\omega_o$). Meanwhile, the contribution of the KAM islands in Fig. 2(b) gives rise to large amplitudes at various frequencies $\omega > \omega_o$. Finally, in this regime we see that as the symmetry breaks, the zero frequency offset value of σ_{xx} becomes larger than that of σ_{yy}, indicating that the electron motion becomes more diffusive in the x direction than the y direction. This is expected, as the $b = 2a$ geometry produces open ''channels'' along the x direction which facilitate diffusion, even in this first regime.

For the *second regime*, take $2R_c/a = 1.2$, $b/a > 2$, and $r = 0.85$. We will focus on the contribution of the chaotic orbits discussed in the previous section, in connection with Fig. 4. In this range of parameters, most of phase space volume is occupied by chaotic trajectories. In Fig. 6(a), we show several traces of $\sigma_{xx}(\omega)$, keeping $2R_c = 1.2a$ and r constants, while changing b/a as indicated there. For $1 < b/a \leqslant 2$, we should mention that there is no appreciable difference from the case of a square geometry, probably due to the fact that as $2R_c$ is comparable to the lattice parameters a and b, the electron scatters more frequently and symmetrically, producing chaotic orbits with characteristic frequency self-averaging to ω_o. When b/a grows, the asymmetry in the lattice structure increases, and b is less comparable to $2R_c$, so that the electron dynamics changes substantially, as shown in Fig. 6(a). We see here that large b/a values produce two prominent features in σ_{xx} at $\omega \approx \omega_o \pm \delta$, which become increasingly apart in frequency for larger b/a. The existence of characteristic frequencies different from ω_o, *even when the trajectories are fully chaotic* [see Fig. 3(b)], are due to the long-term metastability of the nearly-pinned orbits discussed in relation with Fig. 4(b). It is then interesting to see that even though the Poincaré section shows a chaotic map, $\sigma(\omega)$ is able to exhibit this unusual metastable behavior arising from (and made stronger by) the asymmetry in the magnetic modulation landscape. We should stress that even in the case of a rather short τ ($= 3 \times 10^{-12}$ sec in this figure), the metastability is not ''erased'' by the impurity scattering, and is clearly visible in σ_{xx}.

In Fig. 6(b), we keep $2R_c/a = 1.2$ and $b = 4a$, while changing r as indicated in the graph [in this figure, and to

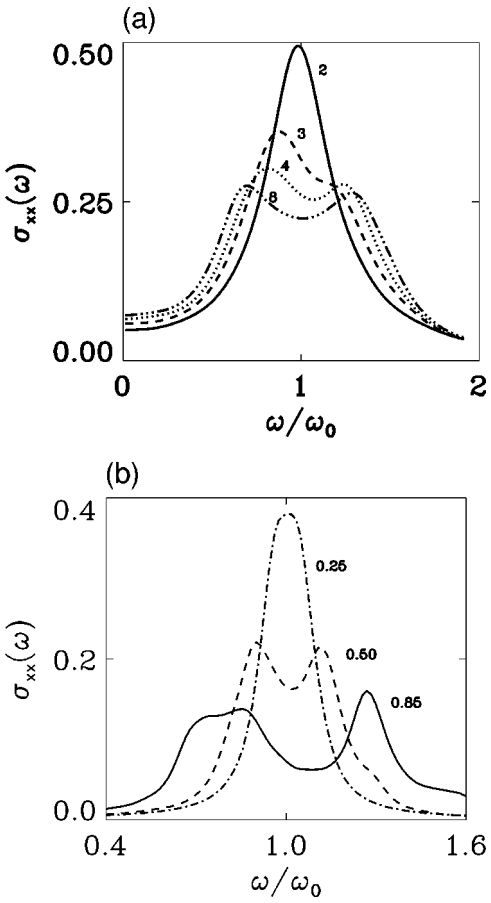

FIG. 6. (a) $\sigma_{xx}(\omega)$ for $2R_c/a = 1.2$, $r = 0.85$, $\tau = 3 \times 10^{-12}$ sec, and $b/a = 2,3,4,8$ as shown. (b) $\sigma_{xx}(\omega)$ shown for $2R_c/a = 1.2$, $b/a = 4$, τ three times longer, and $r = 0.25$, 0.5, and 0.85, as shown.

contrast with Fig. 6(a), we use $\tau = 15 \times 10^{-12}$ sec, three times longer than before]. For weak modulation, $r < 0.5$, the runaway quasiperiodic trajectories and KAM tori do survive and the chaotic trajectories do not cross the wall of maxima in the y direction, as shown earlier in Fig. 3(a). Moreover, the corresponding chaotic trajectory extended along only the x direction will self-average to a frequency $\omega \approx \omega_o$. This can clearly be seen in $\sigma_{xx}(\omega)$ curves which show only a broadening similar to a Drude peak for a uniform field (except for a larger width and flatter top produced by the intrinsic diffusive behavior of the trajectories). As the modulation increases to $r \geqslant 0.5$, we start seeing the single σ peak split into a double peak about ω_o. At $r = 0.85$, where most of the phase space is occupied by a chaotic trajectory, the double peak is clearly developed (in addition to a low-frequency remnant structure from the small quasiperiodic orbits). We should also notice that in this regime the zero frequency offset of σ_{xx} is always larger than that of σ_{yy} (not shown), in agreement with the intuitive notion that the runaway orbits along the x direction contribute more to the dc conductivity, even when the diffusion is fully two dimensional.

In order to further identify the different contributions to the conductivity in this regime, we now calculate the spectrum for a single-orbit, $S_{xx}(\omega)$. This quantity is the contribution to σ_{xx} coming from a single trajectory (i.e., the velocity autocorrelation function for that trajectory). Figure 7 shows S_{xx} for the *same* chaotic orbit but starting at two dif-

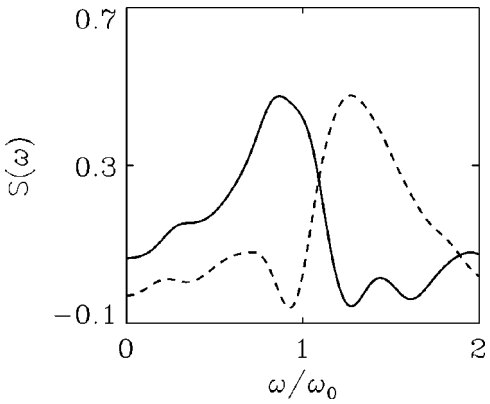

FIG. 7. Single-orbit spectrum $S_{xx}(\omega)$ for the same chaotic trajectory with $2R_c/a=1.2$, $b/a=4$, and $r=0.85$, but starting at different points. Solid trace reflects motion along x channels; dashed trace that between nearest antidots.

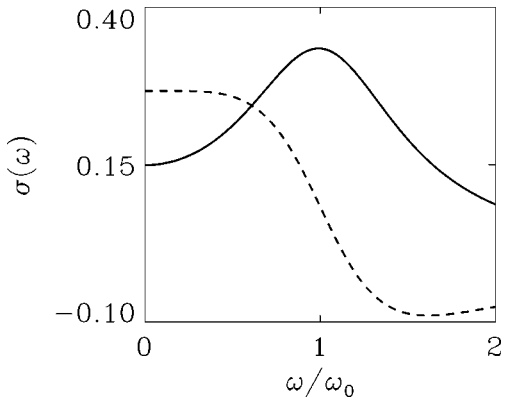

FIG. 8. $\sigma_{xx}(\omega)$ (solid trace) and $\sigma_{xy}(\omega)$ (dashed) for $2R_c=6a$, $b=2a$, and $r=0.56$. xx and yy components are identical.

ferent points on the trajectory. The first trace, appearing solid and with a peak at $\omega\approx 0.9\omega_o$, is obtained when we integrate the dynamics starting at a point in the magnetic landscape identified as a ''channel'' of minima, i.e., the electron motion is mostly diffusive along the x direction (an integration over a 5τ interval is presented). The second curve, dashed and with a peak at $\omega\approx 1.3\omega_o$, was obtained when the integration starts at a point between two nearest antidots (maxima) in the x direction. Notice that here the electron motion was drifting to cross the magnetic barrier in the y direction and formed a short-lived metastable quasiperiodic orbit. It is then further verification that as the particle executes the chaotic trajectory, it is being trapped along channels formed by nearest-neighbor maxima or antidots. This effect is carried through to the frequency-dependent conductivity, even for the short τ used ($=3\times 10^{-12}$ sec).

For the *third regime* of large cyclotron orbits, let us consider $2R_c/a=6$, $b/a=2$, and $r=0.56$. As mentioned in the previous section, the phase space in all these cases is completely occupied by a single chaotic trajectory, even for weak magnetic modulation strength r, and shows no signs of metastability. One typically finds $\lambda=1.14$, the largest Liapunov exponent we found for this regime. We show in Fig. 8 the conductivity curves of $\sigma_{xx}(\omega)$ and $\sigma_{xy}(\omega)$ for the case mentioned. In this example, even though $a\neq b$, we obtain $\sigma_{xx}(\omega)=\sigma_{yy}(\omega)$ due to the strong scattering produced by the modulation, since on the scale of the cyclotron radius the lattice appears basically symmetric. Consequently, the chaotic trajectory averages over all directions, producing a single but much broadened peak at $\omega=\omega_o$ and with a large zero-frequency offset, showing indeed that the motion is fully diffusive in both directions.

V. CONCLUSIONS

We have studied the frequency-dependent magnetotransport in a two-dimensional magnetic field modulation in a rectangular lattice symmetry for various parameter regimes. This study has revealed that a class of resonances exist in the ac conductivity, reflecting the different character of the various electron trajectories, and the degree of integrability (or non-) of these systems. In all cases, we have found a correlation between the dc conductivity $\sigma_{ii}(0)$ and the value of the largest positive Liapunov exponent λ. As λ increases, the zero-frequency offset increases, indicating that the chaotic trajectories become more and more diffusive, even changing diffusive character from one to two dimensional, as the modulation increases. The study of different profiles of magnetic field modulation and even different lattice structures, both theoretically and experimentally, should give us better insights into the microscopic character of the electron trajectories in different regimes. The possible screening effects which would mask some of the frequency dependence discussed here (so-called magnetoplasmon effects[16,17]) are being studied and will be presented elsewhere. It is, however, anticipated that the single-particle features discussed here would persist even when plasmon effects are taken into consideration, as the experiments in Ref. 11 have shown.

ACKNOWLEDGMENTS

We are thankful for discussions with J. Thomas, R. Rollins, and P. Jung. This work has been partially supported by DOE Grant No. DE-F02-91ER45334. S.E.U. acknowledges support by the AvH Foundation.

[1] For reviews see: K. Ensslin and R. Schuster, in *Quantum Dynamics of Submicron Structures*, NATO ASI Vol. 291, edited by H.A. Cerdeira, B. Kramer, and G. Schön (Kluwer, Dordrecht, 1995), p. 247; and D. Weiss, *ibid.*, p. 327.

[2] K. Ensslin and P.M. Petroff, Phys. Rev. B **41**, 12 307 (1990); D. Weiss, M.L. Roukes, A. Menschig, P. Grambow, K. von Klitzing, and G. Weimann, Phys. Rev. Lett. **66**, 2790 (1991); A. Lorke, J.P. Kotthaus, and K. Ploog, Superlattices Microstruct. **9**, 103 (1991).

[3] R. Fleischmann, T. Geisel, and R. Ketzmerick, Phys. Rev. Lett. **68**, 1367 (1992).

[4] J. Wagenhuber, T. Geisel, P. Niebauer, and G. Obermair, Phys. Rev. B **45**, 4372 (1992).

[5] R. Schuster, K. Ensslin, J.P. Kotthaus, G. Böhm, and W. Klein,

Phys. Rev. B **55**, 2237 (1997); S. Lüthi, T. Vancura, K. Ensslin, R. Schuster, G. Böhm, and W. Klein, *ibid.* **55**, 13 088 (1997).

[6] P. Vasilopoulos and F.M. Peeters, Superlattices Microstruct. **7**, 393 (1990); F.M. Peeters and P. Vasilopoulos, Phys. Rev. B **47**, 1466 (1993).

[7] H.A. Carmona, A.K. Geim, A. Nogaret, P.C. Main, T.J. Foster, M. Henini, S.P. Beaumont, and M.G. Blamire, Phys. Rev. Lett. **74**, 3009 (1995); P.D. Ye, D. Weiss, R.R. Gerhardts, M. Seeger, K. von Klitzing, K. Eberl, and H. Nickel, *ibid.* **74**, 3013 (1995); S. Izawa, S. Katsumoto, A. Endo, and Y. Iye, J. Phys. Soc. Jpn. **64**, 706 (1995).

[8] U.J. Gossmann, A. Manolescu, and R.R. Gerhardts, Phys. Rev. B **57**, 1680 (1998).

[9] E. Badran and S.E. Ulloa, Physica B **249-251**, 339 (1998).

[10] G.J.O. Schmidt, Phys. Rev. B **47**, 13 007 (1993); M. Fliesser, G.J.O. Schmidt, and H. Spohn, Phys. Rev. E **53**, 5690 (1996).

[11] E. Vasiliadou, R. Fleischmann, D. Weiss, D. Heitmann, K. von Klitzing, T. Geisel, R. Bergmann, H. Schweizer, and C.T. Foxon, Phys. Rev. B **52**, 8658 (1995).

[12] The introduction of τ guarantees particle diffusion for long times, and suppresses the possible anomalous diffusion and concomitant divergence of $\sigma(\omega)$ for low frequencies. See Wagenhuber *et al.*, Ref. 4. We choose typical values for the scattering time of $\tau \approx 10^{-11}$ sec (or $\hbar/\tau = 66\ \mu$eV, for a relatively good mobility in GaAs of 30 $m^2V^{-1}s^{-1}$), although our conclusions are insensitive to the detailed value of τ, as we illustrate.

[13] A. Wolf, J.B. Swift, H.L. Swinney, and J.A. Vastano, Physica D **16**, 285 (1985).

[14] M.C. Gutzwiller, *Chaos in Classical and Quantum Mechanics* (Springer, New York, 1990).

[15] Notice that since the modulation is magnetic, the particle does not really ''collide'' with maxima, as in the case of an electrostatic modulation. Here, the particle trajectory continually decreases its radius of curvature as it approaches a more intense field, and is then deflected away from it much more smoothly than in the electrostatic/scalar potential case. See, e.g., *The Classical Theory of Fields*, L.D. Landau and E.M. Lifshitz (Pergamon, New York, 1975).

[16] D. Heitmann and J.P. Kotthaus, Phys. Today **46** (6), 56 (1993).

[17] X. Wu and S.E. Ulloa, Phys. Rev. B **47**, 10 028 (1992); S. Mikhailov, *ibid.* **54**, 14 293 (1996).